IEEE Access
Multidisciplinary | Rapid Review | Open Access Journal

Received November 29, 2021, accepted December 30, 2021, date of publication January 4, 2022,
date of current version January 13, 2022.

Digital Object Identifier 10.1109/ACCESS.2021.3140071

Experimental Study on the Influence of Flexible Control on Key Parameters in Reverse Osmosis Desalination

SHUAI CHU[1], SHITAN ZHANG[2], XIAONA MA[3,4], YINXUAN LI[5], DENGGAO QIU[6], WEICHUN GE[1,7], AND LEI KOU[8]

[1]School of Electrical Engineering, Shenyang University of Technology, Shenyang 110870, China
[2]School of Electrical Engineering, Northeast Electric Power University, Jilin 132012, China
[3]Jiangsu Key Laboratory of Marine Bioresources and Environment, Jiangsu Ocean University, Lianyungang 222005, China
[4]Key Laboratory of Experimental Marine Biology, Center for Ocean Mega-Science, Institute of Oceanology, Chinese Academy of Sciences, Qingdao 266071, China
[5]State Grid Tianjin Marketing Service Center (Metrology Center), Tianjin 300010, China
[6]Fisheries Research Institute of Fujian, Xiamen 361013, China
[7]State Grid Liaoning Electric Power Company Ltd., Shenyang 110006, China
[8]Institute of Oceanographic Instrumentation, Qilu University of Technology (Shandong Academy of Sciences), Qingdao 250353, China

Corresponding author: Xiaona Ma (marianna_iocas@163.com)

This work was supported in part by the China Agriculture Research System of the Ministry of Finance (MOF) and the Ministry of Agriculture and Rural Affairs (MARA) under Grant CARS-47, in part by the Special Fund for Marine and Fishery Structure Adjustment in Fujian Province-Development and Application of Physical Treatment Facilities for Wastewater of Seawater Pond under Grant 2021HYJG11, and in part by the National Key Research and Development Program of China under Grant 2019YFB1505400.

ABSTRACT Variable-frequency drive (VFD) has been widely used in reverse osmosis desalination. Our purpose is to study how the VFD and pressure regulating valve affect the key parameters of reverse osmosis desalination and their action principle through experiments. Firstly, the power frequency is controlled by VFD, and the operating pressure is controlled by pressure regulating valve (needle valve) in the experiment. The feed water passes through the multimedia filter, precision filter and permeable membrane channel in turn, and permeate water and brine enter the fresh water tank and the brine tank respectively. Secondly, through experiments on seawater and brackish water respectively, the water flow rate, product water quality, energy consumption and recovery rate under different operating pressures are obtained when the power frequency is 25, 30, 35, 40, 45, and 50 respectively. Finally, combined with the working principle and mathematical model of VFD and high-pressure pump motor, the reason for the experimental results caused by the operation change is explained theoretically. The experimental results verify that for a certain recovery rate, the specific energy consumption required for water production decreases with decreasing power frequency. This provides desalination energy savings but at the expense of permeate production speed.

INDEX TERMS Reverse osmosis, variable-frequency drive, specific energy consumption, recovery rate, power frequency.

NOMENCLATURE

ABBREVIATIONS

BP	booster pump.
BW	brackish water.
ERD	energy recovery device.
HPP	high-pressure pump.
MED	multi-effect distillation.
MSF	multi-stage flash.
PX	pressure exchange.
PX	pressure exchange.
RO	reverse osmosis.
SEC	specific energy consumption.
SW	seawater.
VFD	variable-frequency drive.

PARAMETERS

α	retained salt ratio (%).
β	purge cut-off point.
β_{ERD}	leakage rate of energy recovery device (%).
ΔP	pressure difference of pressure vessel (bar).
Δp_{avg}	average hydraulic pressure difference (bar).

The associate editor coordinating the review of this manuscript and approving it for publication was Binit Lukose.

ΔQ_D the total amount of solution transferred to the draw side (m^3/s).
ρ water density (kg/m^3).
η_{HP} HPP efficiency (%).
η_{intake} mechanical efficiency of water intake pump (%).
η_p overall efficiency of pumps (%).
Φ_m main flux (Wb).
σ constant of solution concentration converted into osmotic pressure.
ε dimensionless relative excess pressure.
φ_1 stator power factor angle (rad).
φ_2 rotor power factor angle (rad).
A water permeability of membrane ($m^3/(m^2 \cdot s \cdot Pa)$).
c_H head coefficient.
c_Q flow coefficient.
c_W power coefficient.
C_T torque constant.
D impeller diameter (m).
E_2' equivalent terminal voltage at rotor side (V).
f power frequency (Hz).
$f_{N,H}$ rated frequency (Hz).
g gravitational acceleration (m/s^2).
H head (m).
$H_{N,H}$ rated head (m).
I_0 excitation current (A).
I_1 stator input current (A).
I_2' rotor side equivalent current (A).
k mass transfer coefficient (m/s).
n motor speed (r/min).
n_1 synchronous speed (r/min).
$n_{N,H}$ rated speed (rad/min).
P motor shaft power (kW).
P_0 osmotic pressure of raw feed water (bar).
p pole pair numbers of motor rotating magnetic field.
P_1 motor input power (W).
P_2 mechanical power output (W).
p_{ad} additional loss (W).
p_{Cu1} stator copper loss (W).
p_{Cu2} rotor copper loss (W).
p_{Fe} stator iron loss (W).
P_{em} electromagnetic power (W).
P_{mec} total mechanical power (W).
P_f feed pressure of RO channel (bar).
P_p permeate pressure (bar).
P_r residual liquid pressure (bar).
$P_{f(plant)}$ plant feed pressure (bar).
$P_{N,H}$ rated power of asynchronous motor (kW).
$P_{N,I}$ rated power of intake pump (kW).
Q flow (m^3/h).
Q_f feed water flow rate (m^3/h).
$Q_{N,H}$ rated flow (m^3/h).
Q_p permeate flow rate (m^3/h).
Q_r residual liquid flow rate (m^3/h).
Q_{bp} booster pump flow rate (m^3/h).
$Q_{f(plant)}$ plant feed flow rate (m^3/h).
Q_{in} intake pump flow rate (m^3/h).
$Q_{p(plant)}$ plant permeate flow rate (m^3/h).
r_1 stator winding resistance Ω.
r_m excitation resistance Ω.
r_2' rotor winding resistance Ω.
RR' volume fraction of feed flow rate.
s slip rate.
T_{em} electromagnetic torque (N·m).
T_2 output torque.
T_0 no-load torque.
Y_{SP} single pass water recoveries (%).
U_1 motor port voltage (V).
$\dot{Q}_p$ permeate production volume (m^3).
$\dot{W}_{in}$ input power (kWh).
η_m motor efficiency (%).
ρ_f feed water density (kg/m^3).
J_w water permeation flux (m^3/m^2s).
Q_{BP} inlet flow rate of booster pump (m^3/h).
$Q_{D,in}$ draw solution influent (m^3/s).
$Q_{F,in}$ feed solution influent (m^3/s).
Q_{HP} inlet flow rate of high pressure pump (m^3/h).
W_{HP} high pressure pump power (kWh).
x_1 stator leakage reactance Ω.
x_2' rotor leakage reactance Ω.

I. INTRODUCTION

As an important natural resource, water is closely related to production and life. Although water resources cover 70% of the Earth's surface, 97.5% of them are too high in salt to be directly consumed by humans [1]. The shortage of fresh water has become a common global crisis [2]–[4]. According to the World Resources Association, the threat of global water shortages is expected to intensify in the next 20 years due to population growth, economic growth and energy consumption.

Seawater desalination is an effective way to increase the fresh water supply and relieve the pressure of fresh water shortages. The desalination capacity is growing rapidly in China and around the world (Figure 1(a)). Tianjin and Shandong Provinces account for 26% and 24% of China's desalination capacity, respectively (Figure 1(b)), and they are the two cities with the largest desalination capacity in China. The Middle East is starved of fresh water and has the largest desalination capacity in the world (Figure 1(c)). Commonly used desalination technologies include SWRO, MSF and MED. With the emergence of PX energy recovery devices, the SEC of RO is significantly lower than that of other desalination technologies [5], [6]. RO is currently the most popular and widely method to provide sustainable freshwater [7]–[9].

In RO desalination technology, water molecules are squeezed through the membrane, and solid particles are blocked at the feed water side. The electricity cost accounts for 44% of the total cost and is the main contributor to

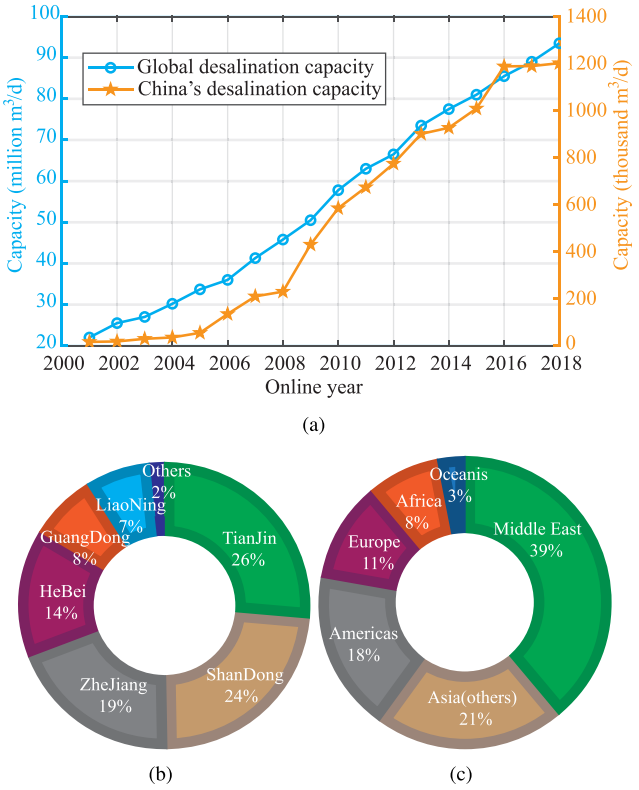

FIGURE 1. Installation capacity and distribution of seawater desalination. (a) Installation capacity of desalination in China and the world in recent years. (b) Distribution of the desalination capacity in China. (c) Distribution of global desalination capacity. [10].

the desalination operating cost [11]–[13]. Minimizing power consumption is the most effective way to reduce operating costs. The complete RO desalination process includes four steps: water intake, pretreatment, reverse osmosis treatment and posttreatment. Reverse osmosis treatment accounts for approximately 71% of the energy consumption of the whole process, followed by water intake (there may be some differences in energy consumption due to the influence of the water source location.) [14]. The power consumption of reverse osmosis treatment is greatly affected by the recovery rate. When the recovery rate is high, the specific energy consumption of SWRO rises sharply, and the osmotic membrane reaches the pressure limit. Therefore, the recovery rate of SWRO desalination shall not exceed 60% [15]. The energy consumption of BWRO is lower than that of SWRO, and the recovery rate can reach more than 80% [16], [17].

The effect of SWRO equipment performance on energy consumption has been widely studied through theoretical modeling and experimental analysis [18]–[23]. With the high penetration of wind power and photovoltaic in the power grid, the current trend is that desalination plants need to operate flexible enough to cope with the volatility of wind and solar energy. The power electronic VFD is a tried-and-tested, reliable and cost-effective solution that ensures precise control of torque and speed for electric rotating machines (such as pumps, compressors, fans, extruders, etc.) in a wide range of industrial fields. VFD provides more efficient energy management and better process control accuracy and flexibility [24]. At present, large-scale RO desalination plants are usually equipped with VFDs and pressure regulating valves. Operators can control water flow [25], energy consumption [26] and recovery rate [27] by adjusting power frequency and operating pressure. Although there is hope and affirmation for the feasibility of long-term operation of RO system under variable load, the work reported in [28]–[31] is qualitative, and no specific dynamic model has been developed for the analysis of RO system under variable conditions.

For different application scenarios, Table 6 lists the most recently used SEC calculation formula. Although these scholars have made great contributions to their work and inspired our interest in further research, the current research does not consider the perfect detailed RO model to analyze the results of different operating conditions, nor does it consider the operation optimization of the system. For example, parameters such as the polarization factor [32] change with changes in operating conditions, or the efficiency of the VFD decreases at a frequency lower than its rated maximum frequency. The purpose of this paper is to study the effects of changing SWRO operating conditions on energy consumption, recovery and product water quality through experiments. The main contributions of this paper are as follows:

- The key parameters (feed water flow rate, permeate flow rate, brine flow rate, permeate quality, total energy consumption, recovery rate and SEC) of RO desalination are studied by experiments.
- The energy transfer relationship of RO desalination is analyzed. The working principle of the energy consumption change caused by the VFD and pressure regulating valve is studied.
- The relationship between the SEC, recovery rate and power frequency is analyzed. It is proven that reducing the power frequency has a positive impact on reducing energy consumption, especially for BWRO, but reduces the permeate production speed.

The organizational structure of this paper is as follows. The experimental study of SWRO and BWRO is presented in Section II. Section III discusses the experimental process and results, and the conclusions are summarized in Section IV.

II. EXPERIMENT

A. EXPERIMENTAL EQUIPMENT

The rated permeate water production capacity of RO desalination equipment is 5 m^3/day (Figure 2). Table 1 lists the main components of the experimental equipment: the water storage tank, water pump, VFD, filtration system and RO membrane. The RO membrane limits the operating pressure of the system so that it cannot exceed 6 MPa. Although the experimental equipment contains flowmeters, two electronic

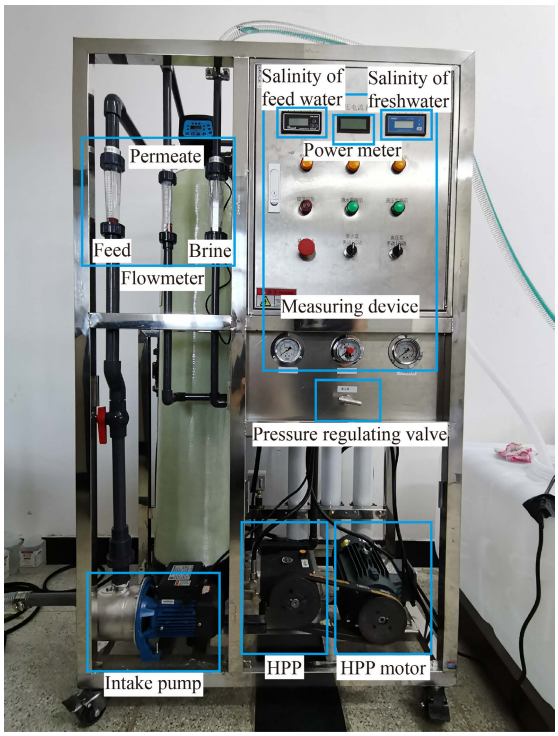

(a) Front view of the device.

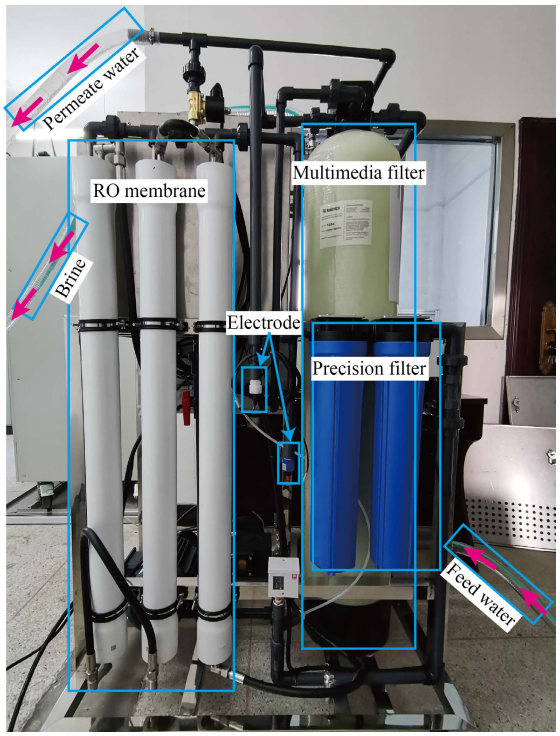

(b) Photo of the back of the device.

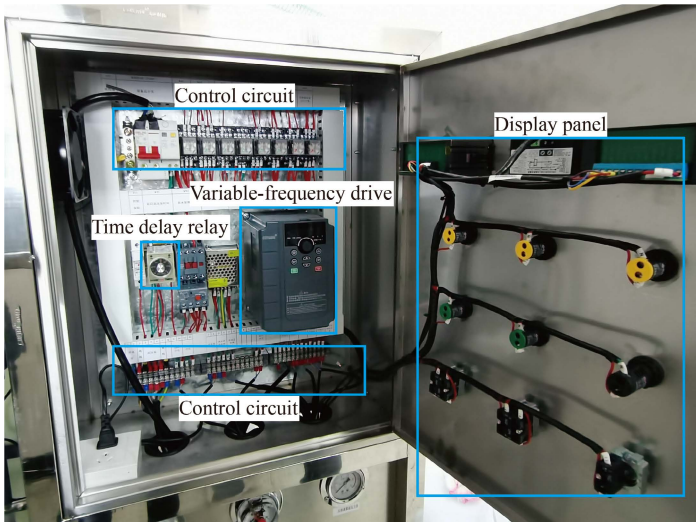

(c) Internal photo of display panel.

FIGURE 2. View photos of the device from different angles.

scales are used to accurately measure the weight of the permeate water tank and brine tank. The permeate water tank and brine tank are placed on electronic scales to accurately measure permeate production and brine production, respectively. In addition, the VFD can adjust the speed of the asynchronous motor by changing the power frequency. The wiring mode of VFD control circuit is shown in Figure 3. The speed of the motor is proportional to the frequency of the power supply. Equation (1) defines the relationship between the motor speed and power frequency. The HPP and the asynchronous motor are connected through a conveyor belt, and the HPP and asynchronous motor have the same speed.

$$n = 60f/p \tag{1}$$

The operation process of the experimental equipment is shown in Figure 4. First, the intake pump delivers feed water from the feed water tank to multiple media filters for pretreatment. Then, the filtered water passes through a 5-micron precision filter and a 1-micron precision filter in turn. To avoid the RO membrane being scratched, suspended solids greater

TABLE 1. Calculation formulas of SEC used in recent years.

Components	Specifications	Function
Feed water tank	400 L	Guaranteed water supply of the later stage
Permeate water tank	200 L	Storage of permeate water
Brine tank	400 L	Storage of brine
Rinse tank	25 L	Backwashing the reverse osmosis membrane
Intake pump	$P_{N,I} = 0.37$ kW	Take water from the feed water tank
HPP	15 L/min	Increase water pressure to RO membrane
Asynchronous motor	$P_{N,H} = 1.5$ kW $\eta_{e,hp} = 82.8\%$	Drive HPP
VFD	TD500-T0022G3	Adjust the speed of the asynchronous motor
Pressure regulating valve	-	Adjust the RO operating pressure
Multimedia filter	1252	Interception of suspended solids greater than 40 μm
Precision filter	20 in	Filter the suspended solids of more than 1 μm to avoid scratching the RO membrane
RO membrane	2540	Remove salt, suspended particles, colloids and microorganisms in water

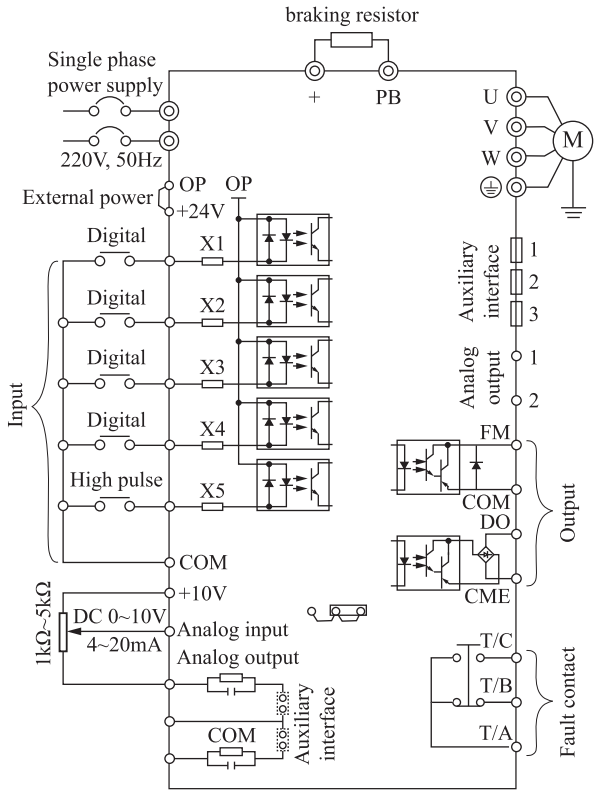

FIGURE 3. The wiring mode of VFD control circuit.

than 1 micron in water are filtered out. Finally, the filtered water is pressurized by an HPP and transported to the RO membrane to remove salt, suspended particles, colloids and microorganisms in the water. The permeate enters the permeate water tank, and the brine enters the brine tank.

B. EXPERIMENTAL CONDITION

The conditions and hypotheses involved in the experiment are listed below.

- The feed water tank is equipped with a constant temperature heating rod. The feed water temperature is constant at 20 °C.
- The composition of seawater is very complicated. The contents of chemical elements in seawater vary greatly (Figure 5). According to the composition and proportion of the seawater in Dalian Bay, $NaCl$, $MgCl_2$, $CaCl_2$, KCl and $MgSO_4$ compounds were added into the water as the experimental feed water.
- The biofouling, suspended solids and inorganic contaminants on the membrane surface are considered constant in a short time.
- It is assumed that the desalination capacity of the RO desalination equipment will not change in a short period of time.
- The PX energy recovery device is only suitable for large-scale desalination plants. Because the scale of the experimental equipment is small in this paper, a PX energy recovery device and booster pump are not installed (which will not affect the conclusion of the experiment).

Within the allowable range of safe operation of the experimental equipment, the permeate water quality, power consumption and recovery rate are studied by changing the power frequency and operating pressure. The operation parameters of the experimental process are set as shown in Table 2. The rated speed and frequency of the asynchronous motor are 1400 r and 50 Hz, respectively. According to (1), when the power frequency is reduced from 50 Hz to 25 Hz, the speed of the motor is also reduced to half of the rated speed. Before the start-up of the experimental equipment, the power frequency of the VFD is set. After the HPP is started, the operating pressure is set by adjusting the pressure regulating valve. After the water production becomes stable, the weight of the electronic scale is recorded immediately and again two minutes later. Therefore, the water production in two minutes is the difference between the value recorded later and the

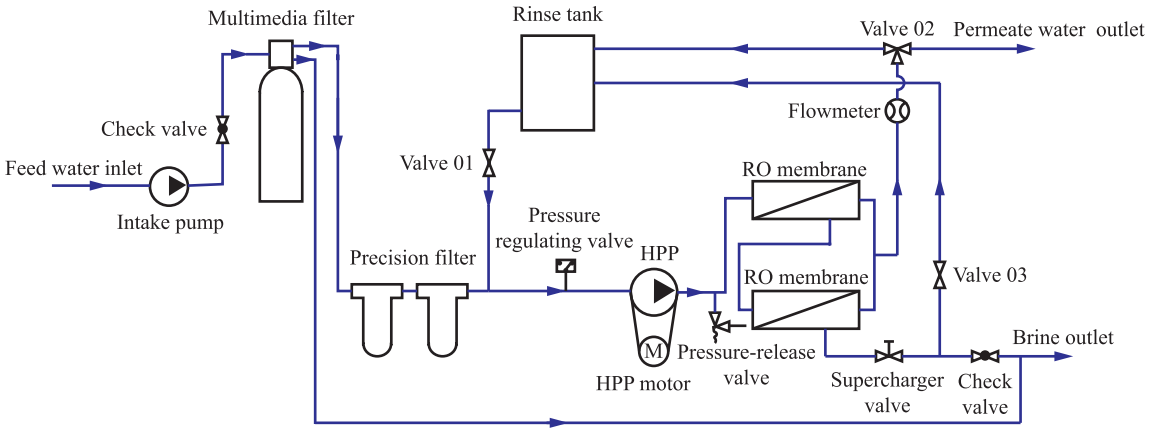

FIGURE 4. Technological process of the RO desalination equipment. To ensure the accuracy of the experimental results, there is no backwash during the experiment. All valves (01, 02, and 03) connected to the rinse tank are closed during the experiment. All permeates flow directly into the permeate water tank.

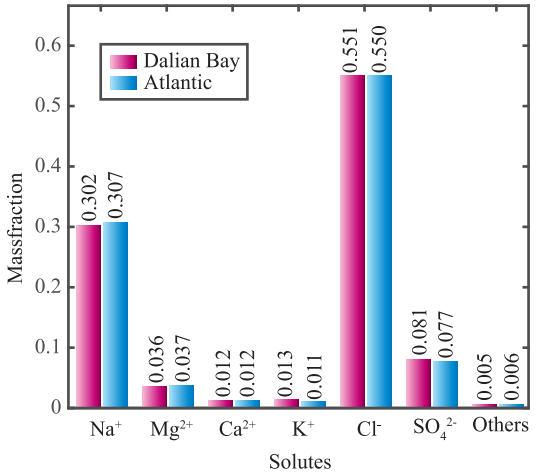

FIGURE 5. Composition and content of particulate matter in seawater. Dalian Bay is located in the southernmost Bay of the Liaodong Peninsula in China. The composition of seawater in Dalian Bay comes from the water quality analysis report in May 2019. Millero *et al.* provided the sea salt composition of the Atlantic surface water [33].

previous value. The detailed experimental flow chart is shown in Figure 6.

C. EXPERIMENTAL RESULT

The VFD adjusts the power frequency to change the motor speed. The HPP always maintains a synchronous speed with the motor. It should be pointed out that the speed of HPP determines the feed water flow rate, and the operating pressure does not change the feed water flow rate. Therefore, when the power frequency is determined, the feed water flow rate does not change. In the experiment, the feed water flow rate is given in Table 3.

Both the HPP speed and pressure affect the permeate flow rate and the brine flow rate (Figure 7). With increasing power frequency (25 Hz to 50 Hz), the speed of the HPP also increases. Then, the permeate production increases slightly, and the output of brine increases significantly. The growth

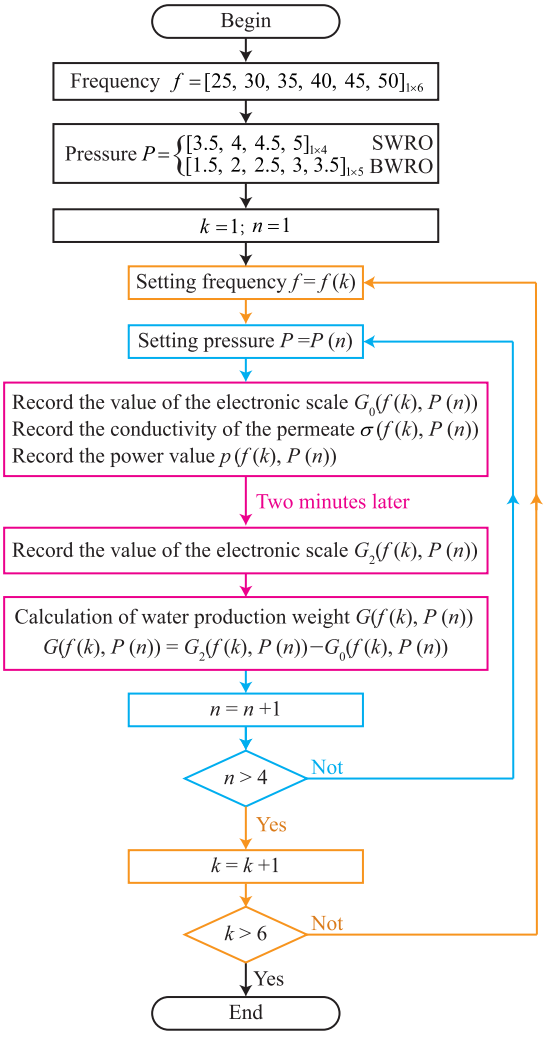

FIGURE 6. Experimental operation flow chart of RO desalination.

rate of the brine flow rate is always higher than that of the permeate. In addition, the pressure regulating valve increases the operating pressure by limiting the brine flow. When the

TABLE 2. Experimental parameters of RO desalination.

Parameter	Seawater	Brackish water
Temperature (°C)	20	20
Salt concentration (mg/L)	35, 000	3500
Pressure (MPa)	[3.5, 4.0, 4.5, 5.0]	[1.5, 2.0, 2.5, 3.0, 3.5]
Power frequency (Hz)	[25, 30, 35, 40, 45, 50]	[25, 30, 35, 40, 45, 50]

TABLE 3. Feed water flow of SWRO and BWRO at different power frequencies (kg/min).

Power frequency (Hz)	Seawater	Brackish Water
25	7.04	7.06
30	8.51	8.50
35	9.89	9.90
40	11.51	11.51
45	12.90	12.91
50	14.50	14.48

pressure increases by 0.5Mpa, the weight of permeate in the SWRO and BWRO experiments increases by 1.1kg and 2kg, respectively. When the operating pressure and power frequency reach a maximum (SWRO (5.0 MPa, 50Hz), BWRO (3.5 MPa, 50Hz)), the flow rate of the permeate reaches a maximum.

There is a strong linear relationship between the water conductivity and salt content. A higher conductivity indicates that there is a higher salt content in the permeate. The HPP speed and pressure have a great influence on the RO filtration efficiency (Figure 8). In SWRO, because the feed water salinity is very high, increasing the operating pressure can always reduce the conductivity of permeate. In addition, increasing the HPP speed also significantly improves the permeate quality (Figure 8(a)). At any operating pressure, the conductivity at 50 Hz is always approximately 0.3 mS/cm lower than that at 25 Hz. However, the conductivity tends to be stable in BWRO when the frequency is higher than 40 Hz (Figure 8(b)). At this time, the HPP speed and pressure have little effect on the BWRO filtration efficiency. The filtration capacity of the RO membrane reaches the limit. Although the HPP speed and pressure affect the desalination rate, the filtration efficiencies of SWRO and BWRO are always more than 95% and 99%, respectively.

Higher HPP speed and pressure consume more power (Figure 9). This power includes the total power of the asynchronous motor, intake pump and other auxiliary equipment. The power consumption of SWRO is much higher than that of BWRO. The additional energy consumption mainly comes from the asynchronous motor in RO treatment. The energy consumption of the asynchronous motor increases substantially with increasing operating pressure and power frequency. The power consumption of the intake pump and other auxiliary equipment is affected very little by the operating pressure and power frequency.

The inlet pressure is provided by the intake pump (Figure 10). The inlet pressure is independent of the operating pressure provided by the HPP. With increasing power frequency and HPP speed, the inlet pressure decreases gradually. Because the osmotic pressure of seawater is higher than that of brackish water, the inlet pressure of SWRO is higher.

When the recovery rate is too high, the RO membrane is prone to scaling and overconcentration polarization in SWRO. Therefore, a higher recovery rate is considered in the BWRO experiment. The recovery rate is affected by both the operating pressure and power frequency (Figure 11). When the power frequency is low, the low HPP speed reduces the flow rate. At this time, water molecules are no longer overcrowded when passing through the osmotic membrane, and the obstruction degree of membrane impedance to permeate flow is reduced. Therefore, reducing the power frequency is helpful to improve the recovery rate. In addition, the operating pressure is the decisive factor in changing the recovery rate. With the increase of pressure, the recovery rate increases greatly. When the power frequency is 50 Hz, the average recovery rates of SWRO and BWRO increase by 4% and 7%, respectively, for every 1 MPa increase in operating pressure. When the power frequency is low, the recovery rate increases more. When the frequency is 25 Hz and the pressure is 5 MPa, the recovery rates of SWRO and BWRO reach the highest points of 33.3% and 83.5%, respectively. In short, a higher pressure and lower frequency can improve the recovery rate.

The SEC is defined as the electrical energy required to produce each ton of permeate. The SEC has a strong correlation with the operation mode of HPP. The SEC in Figure 12 is obtained from the actual HPP energy consumption measurement. The energy consumption of the intake pump and other auxiliary equipment is not considered. When the power frequency is 25 Hz and the operating pressure is the maximum, the SEC of SWRO and BWRO is the lowest, which are 6.59 kWh/m^3 and 2.01 kWh/m^3, respectively. The SEC under opposite operating conditions (50 Hz) exceeds twice its minimum value. For both SWRO and BWRO, the SEC can be reduced by increasing the operating pressure and reducing the power frequency.

III. DISCUSSION

A. ENERGY TRANSFER

Energy is the consumable of RO desalination. First, the electric energy in the power grid changes the frequency through the VFD. Then, electrical energy is transferred to an asynchronous motor and converted into mechanical energy.

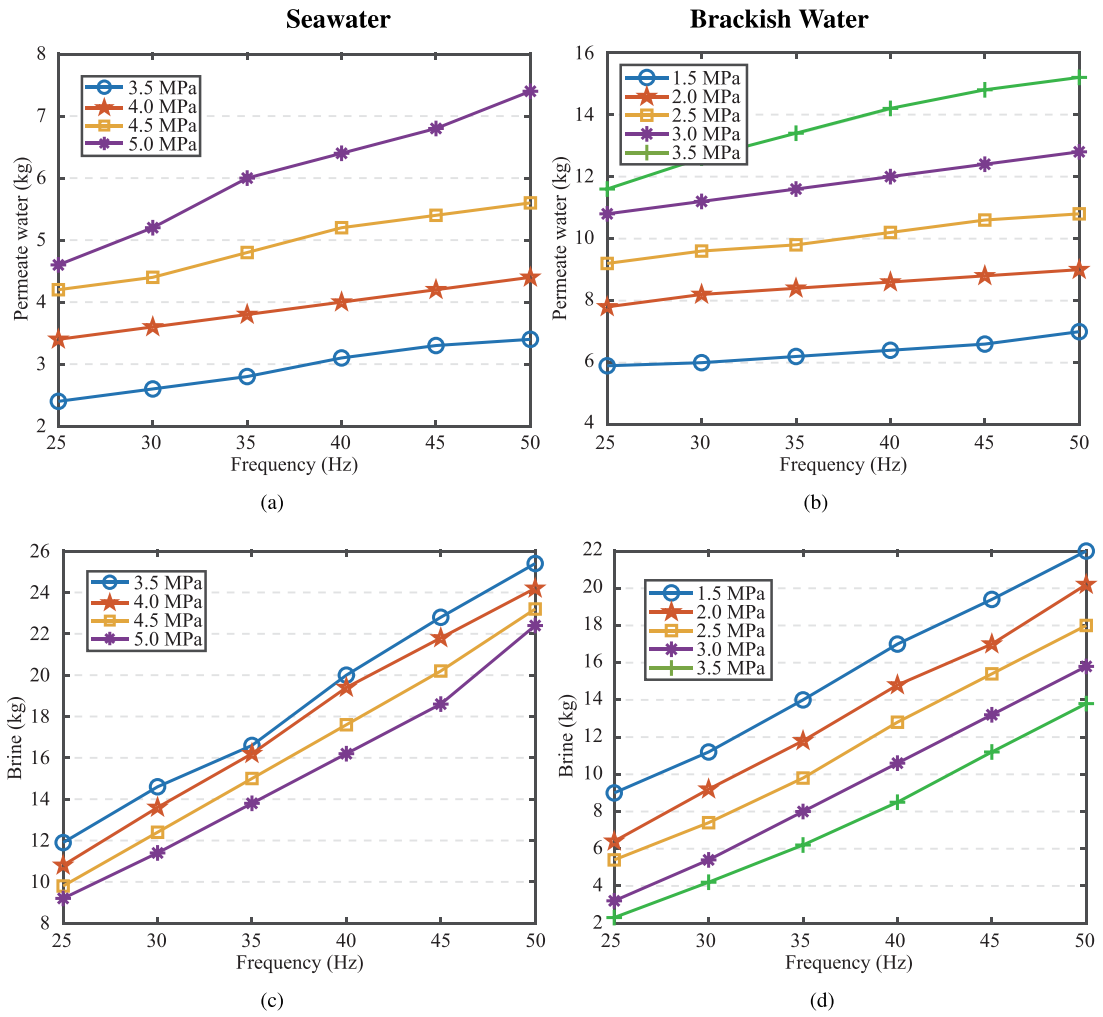

FIGURE 7. Statistical results of the permeate weight and brine weight every two minutes at different pressures and frequencies. (a) Permeate water for SWRO. (b) Permeate water for BWRO. (c) Brine for SWRO. (d) Brine for BWRO.

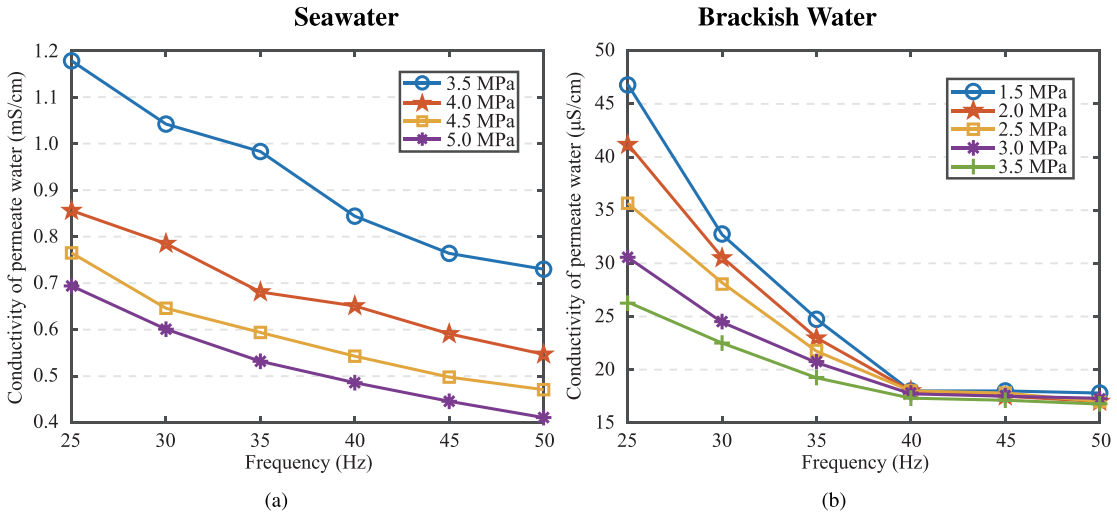

FIGURE 8. Conductivity of the permeate. (a) Conductivity of permeate water for SWRO. (b) Conductivity of permeate water for BWRO.

Finally, mechanical energy is used to drive the HPP. In the process of energy transmission, the asynchronous motor and HPP produce some energy loss (Figure 13). The efficiency of the motor is the ratio of the output mechanical power and input power, as show in (2). The efficiency of the HPP is the ratio of the effective power and input shaft power, as show

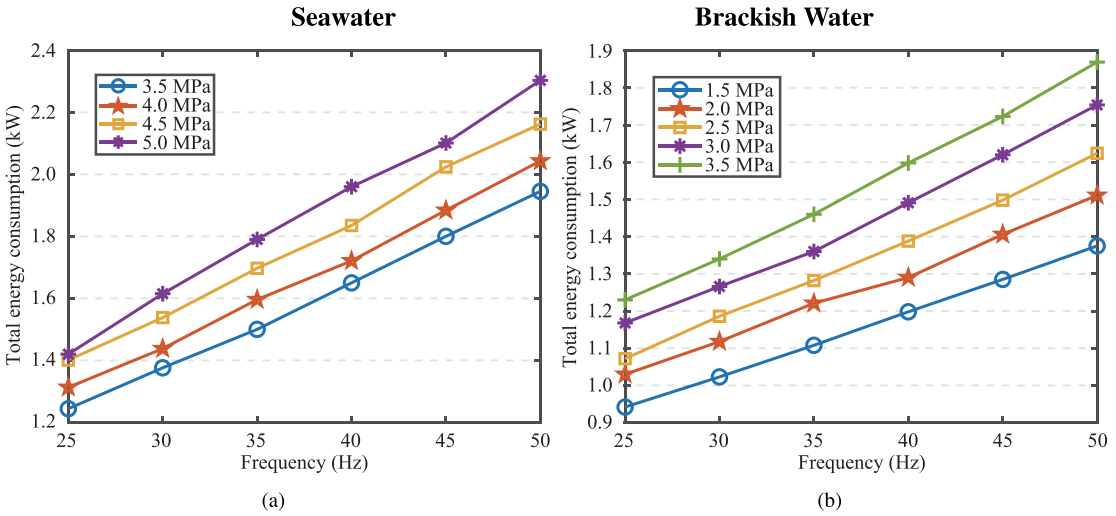

FIGURE 9. Total power demand of RO desalination. (a) Total energy consumption for SWRO. (b) Total energy consumption for BWRO.

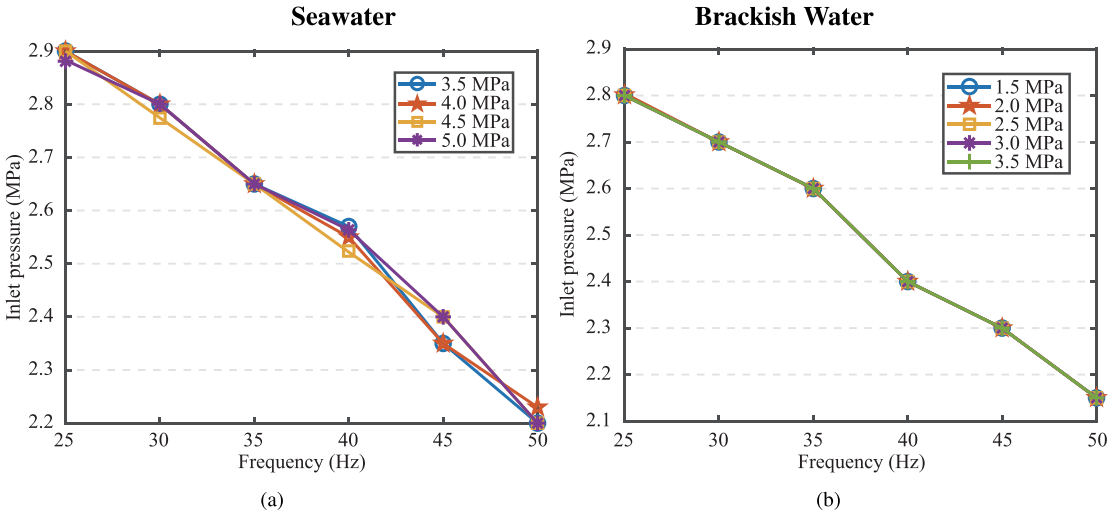

FIGURE 10. Inlet pressure provided by intake pump. (a) Inlet pressure for SWRO. (b) Inlet pressure for BWRO.

in (3). In addition, the friction loss of the belt is very small and can be ignored, so $P_3 \approx P_2$. Therefore, the calculation of SEC under thermodynamic limit constraints needs to consider the efficiency of the motor and HPP and ignore the friction loss of the belt.

$$\eta_m = \frac{P_2}{P_1} \times 100\% \tag{2}$$

$$\eta_{HP} = \frac{P_4}{P_3} \times 100\% \tag{3}$$

The T-type equivalent circuit in Figure 14 can fully reflect the relationship among current, power and torque in asynchronous motor. Therefore, T-type equivalent circuit is used to analyze the power balance relationship of asynchronous motor. When the asynchronous motor is running, the electrical power is input from the power grid and the mechanical power is output from the motor shaft. The input power is shown in (4).

$$P_1 = 3U_1 I_1 \cos\varphi_1 \tag{4}$$

When the motor stator inputs current I_1, copper loss p_{Cu1} will be generated on the stator winding resistance. In addition, the three-phase current generates a rotating magnetic field in the stator winding and cuts the stator core, resulting in stator iron loss p_{Fe}, as shown below.

$$p_{Cu1} = 3I_1^2 r_1 \tag{5}$$

$$p_{Fe} = 3I_0^2 r_m \tag{6}$$

After deducting the stator copper loss p_{Cu1} and stator iron loss p_{Fe} from the motor input power P_1, the remaining power is the electromagnetic power P_{em} transferred from the stator side to the rotor side by the air gap magnetic field through the

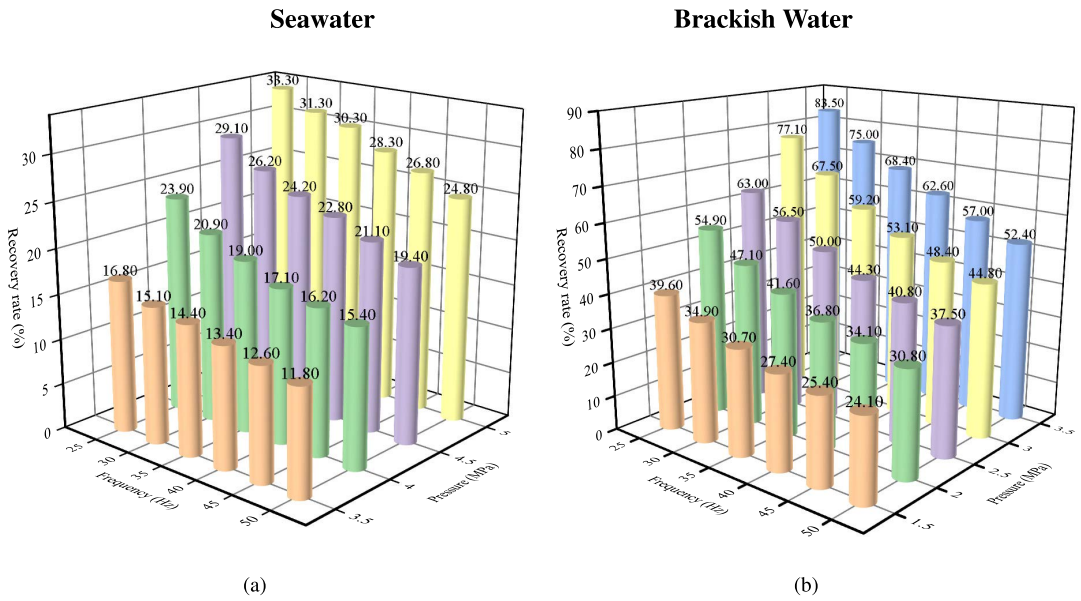

FIGURE 11. Recovery rate under different HPP operation modes. (a) Recovery rate for SWRO. (b) Recovery rate for BWRO.

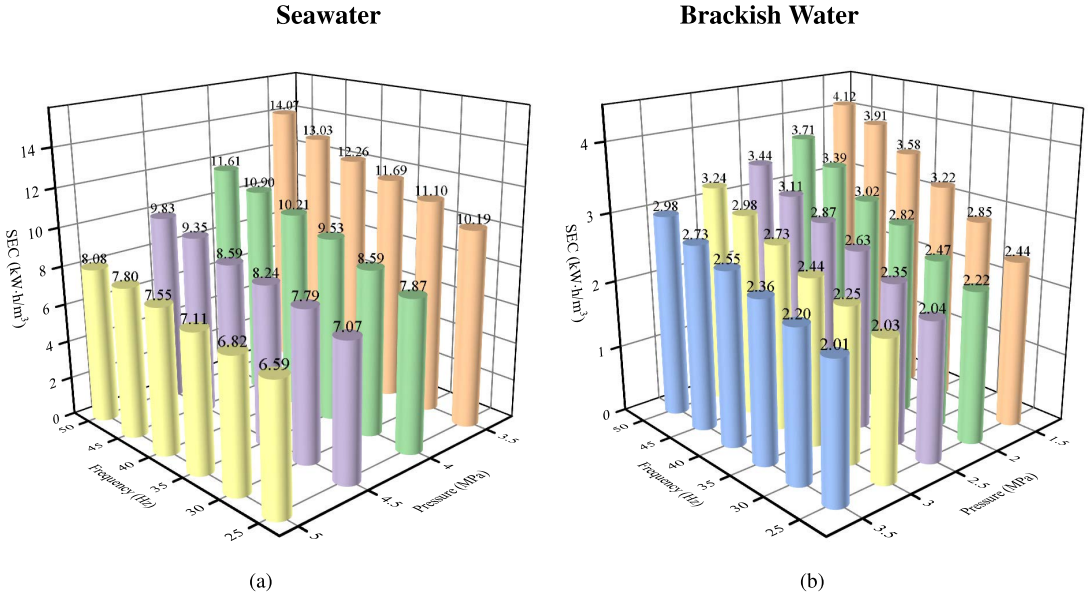

FIGURE 12. SEC under different HPP operation modes. (a) SEC for SWRO. (b) SEC for BWRO.

electromagnetic induction relationship, as shown in (7).

$$P_{em} = P_1 - (p_{Cu1} + p_{Fe}) \tag{7}$$

According to the equivalent circuit physical parameter relationship in Figure 14, the electromagnetic power P_{em} can also be expressed as follows:

$$P_{em} = 3E_2'I_2'\cos\varphi_2 = 3I_2'^2\frac{r'_2}{s} \tag{8}$$

Because the rotor frequency is too low, the iron loss of the rotor can be ignored. The rotor copper loss is the resistance loss caused by the rotor current flowing through the rotor winding.

$$p_{Cu2} = 3I_2'^2 r_2' = sP_{em} \tag{9}$$

Then the total mechanical power on the motor shaft is as follows:

$$P_{mec} = P_{em} - p_{Cu2} = (1-s)P_{em} \tag{10}$$

In addition, when the motor is running, mechanical loss p_{mec} and additional loss p_{ad} are generated. The mechanical power output P_2 on the motor shaft is shown in (11):

$$P_2 = P_{mec} - (p_{mec} + p_{ad}) \tag{11}$$

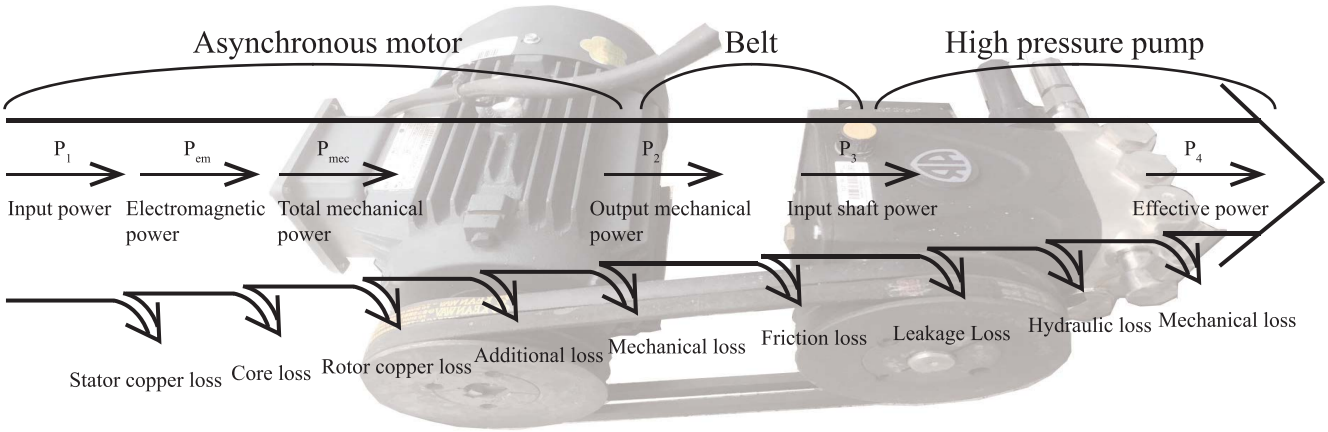

FIGURE 13. Energy transfer process between an asynchronous motor and a high-pressure pump.

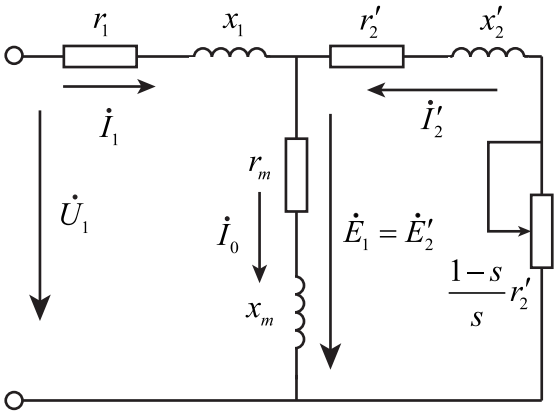

FIGURE 14. T-type equivalent circuit of the asynchronous motor.

From the dynamics, it is known that the mechanical power of the rotating body is equal to the product of the torque acting on the rotating body and the mechanical angular velocity. The left and right ends of (11) are divided by the mechanical angular velocity at the same time. Equation (11) is rewritten as follows.

$$\frac{P_2}{\Omega} = \frac{P_{mec}}{\Omega} - \frac{p_{mec} + p_{ad}}{\Omega} \tag{12}$$

According to the relationship between physical quantities, (12) is equivalent to (13).

$$T_2 = T_{em} - T_0 \tag{13}$$

Mechanical angular velocity $\Omega = 2\pi n/60$. Therefore, the electromagnetic torque in (13) can be simplified as follows.

$$T_{em} = \frac{P_{mec}}{\Omega} = \frac{(1-s)P_{em}}{2\pi\frac{(1-s)n_1}{60}} = \frac{P_{em}}{\Omega_1} \tag{14}$$

Considering the physical characteristics of electromagnetic torque, when $P_{em} = 3E_2'I_2'\cos\varphi_2$, the physical expression of electromagnetic torque is as follows. In (15), C_T is the torque constant, and $C_T = 4.44/2\pi \times 3pN_1K_{N1}$. It can be seen that the electromagnetic torque of the motor increases with the increase of the active component of the current.

$$T_{em} = \frac{P_{em}}{\Omega_1} = \frac{3E'_2I'_2\cos\varphi_2}{2\pi n_1/60} = C_T\Phi_m I_2'\cos\varphi_2 \tag{15}$$

According to Figure 14, the rotor current is calculated as follows:

$$I'_2 = \frac{U_1}{\sqrt{(r_1 + r'_2/s)^2 + (x_1 + x'_2)^2}} \tag{16}$$

Therefore, when $P_{em} = 3I'^2_2 r'_2/s$, the electromagnetic torque can also be expressed in the form of (17). Therefore, when the electromagnetic torque is constant, the terminal voltage of the motor increases with the increase of the power frequency.

$$T_{em} = \frac{P_{em}}{\Omega_1} = \frac{3pU_1^2 r'_2/s}{2\pi f_1[(r_1 + r'_2/s)^2 + (x_1 + x'_2)^2]} \tag{17}$$

Although increasing the power frequency and operating pressure both increase the power consumption (Figure 12), the reasons for the increase in power consumption are different. Next, we analyze the function and principle of the VFD and pressure regulating valve in the RO desalination process to more clearly understand the causes of energy consumption changes.

1) VFD

The VFD is a dual variable output system that includes the output frequency and output voltage. The output frequency of the VFD determines the output voltage, which is proportional to the output frequency. When the motor runs below the fundamental frequency ($\leqslant$ 50 Hz), the motor has a constant torque output. At this time, the output power of VFD is shown in (18).

$$P_1 = \frac{T_{em}n}{9550} = \frac{6T_{em}f}{955p} \tag{18}$$

TABLE 4. Output voltage of VFD (V).

Power frequency (Hz)	SWRO	BWRO
25	197	197
30	234	234
35	271	271
40	307	307
45	345	345
50	383	383

In the water supply equipment driven by VFD, the frequency f determines the speed n of the motor. For the same pump, the proportional law of the pump can be used to calculate the head, flow and power at different speeds [26], [34]. When the impeller diameter is fixed and the speed is changed, the change law of its performance is shown in (19).

$$\begin{cases} \dfrac{Q_{N,H}}{Q} = \dfrac{n_{N,H}}{n} \\ \dfrac{H_{N,H}}{H} = \left(\dfrac{n_{N,H}}{n}\right)^2 \\ \dfrac{P_{N,H}}{P} = \left(\dfrac{n_{N,H}}{n}\right)^3 \end{cases} \tag{19}$$

It can be seen from (1) that the power supply frequency f of the motor is directly proportional to the speed n. Therefore, the frequency f also has the above n-th power (n = 1,2,3) proportional relationship with flow, head and motor shaft power, as shown in (20).

$$\begin{cases} \dfrac{Q_{N,H}}{Q} = \dfrac{f_{N,H}}{f} \\ \dfrac{H_{N,H}}{H} = \left(\dfrac{f_{N,H}}{f}\right)^2 \\ \dfrac{P_{N,H}}{P} = \left(\dfrac{f_{N,H}}{f}\right)^3 \end{cases} \tag{20}$$

Hellmann *et al.* [35] suggested using VFD as an energy-saving method for desalination. Compared with flow control valves, VFDs have the advantage of significantly reducing energy consumption during low flow and pressure. The parameters related to pump performance can be divided into three dimensionless factors, namely head, flow and power coefficient, as shown in (21).

$$\begin{cases} c_H = \dfrac{gH}{f^2D^2} \\ c_Q = \dfrac{Q}{fD^3} \\ c_W = \dfrac{W_{HP}}{\rho f^3 D^5} \end{cases} \tag{21}$$

Constant output torque ensures that the current does not change when the power frequency is lower than the fundamental frequency. At this time, the output voltage increases with increasing output frequency, as shown in (17). In the experiment, the output voltage of the VFD at different power frequencies is given in Table 4.

TABLE 5. Single-phase current active component (A).

Operating pressure (MPa)	SWRO	BWRO
1.5	-	0.75
2.0	-	0.86
2.5	-	0.98
3.0	-	1.11
3.5	1.24	1.24
4.0	1.34	-
4.5	1.44	-
5.0	1.54	-

2) PRESSURE REGULATING VALVE

The needle valve is used as the pressure regulating valve in the experiment. The pressure regulating valve is installed at the brine outlet of the RO channel. The pressure regulating valve cannot change the feed water flow rate. The pressure regulating valve limits the brine flow in the process of increasing the operating pressure. At this time, both the permeate flow rate and recovery rate increase. The brine flow rate is limited, which is equivalent to increasing the load of the HPP. The output torque of the motor is determined by the load. As the load increases, the motor needs to output more torque. The electromagnetic torque of the asynchronous motor is produced by the interaction between the main flux of the air gap and the rotor current active component. The electromagnetic torque T_{em} is proportional to the current active component $I'_2 \cos\varphi$, as shown in (15). In addition, the port voltage of the motor remains constant when the power frequency is determined. Therefore, the energy consumption increases with increasing current active component. The experimental power supply is a three-phase alternating current, and the single-phase current active component in the experiment is given in Table 5.

It should be pointed out that the power loss of the asynchronous motor is related to its port voltage. Higher supply voltage leads to an increase in rotor current and a slight increase in power loss. Moreover, even if the motor output torque is constant, the power supply current increases slightly due to the additional power loss. Therefore, by using VFD to adjust the power frequency, the efficiency of the motor also changes. However, for high-efficiency motors, the change in efficiency is very limited.

B. RELATIONSHIP BETWEEN THE RECOVERY RATE AND SEC

With the development of RO technology, large-scale RO desalination plants are gradually installed with a VFD. The VFD can adjust the power frequency to change the HPP speed to adjust the recovery rate (Figure 11). In past studies, we have fully considered the effects of the recovery rate, brine temperature and salinity on the energy consumption (Table 6), but consideration of the power frequency is lacking. In the experiment, the influence of the power frequency on the recovery rate and SEC of RO desalination was studied when

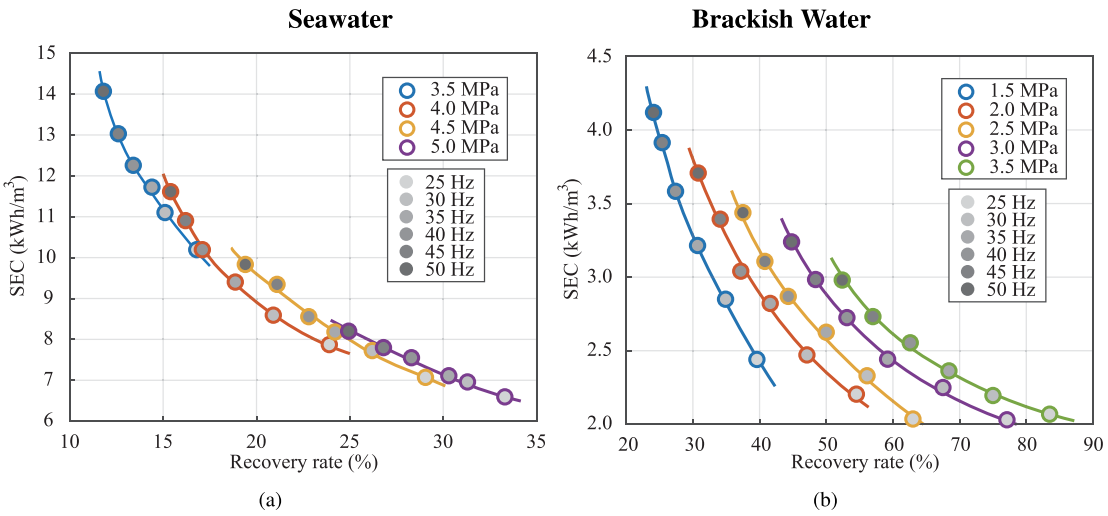

FIGURE 15. SEC vs recovery rate for SWRO and BWRO at different power frequencies and pressures. (a) SWRO. (b) BWRO.

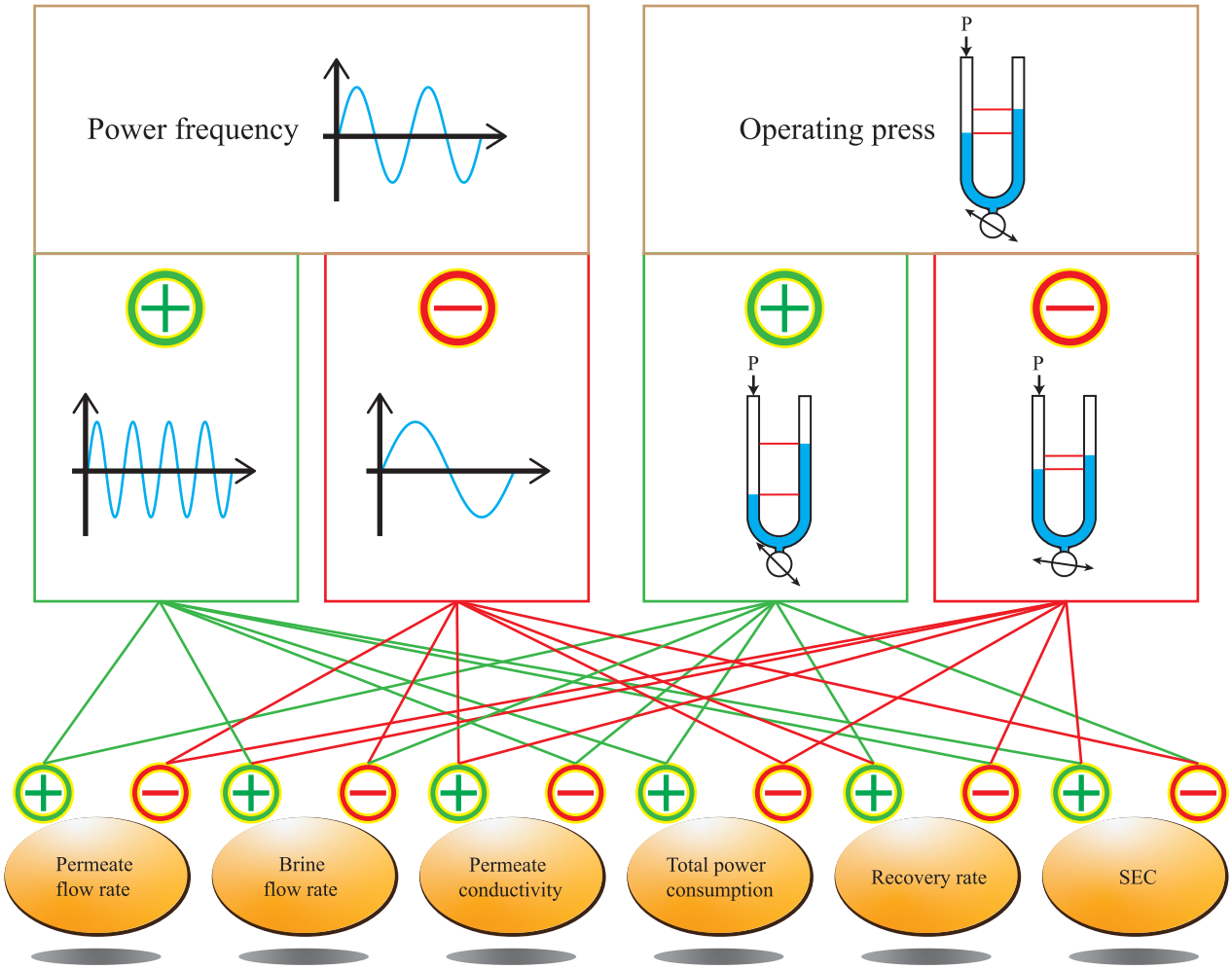

FIGURE 16. Influence of the VFD and pressure regulating valve on the key parameters of RO desalination.

the motor was running below the fundamental frequency ($\leqslant$ 50 Hz). The relationship between the recovery rate and SEC of RO desalination under different operation modes of HPP is given in Figure 15. When the power frequency, feed water concentration and temperature are determined, there is a one-to-one corresponding functional relationship between the SEC and recovery rate. That is, as long as the recovery rate is known, the corresponding SEC can be obtained.

TABLE 6. Calculation formulas of SEC used in recent years.

Specific energy consumption		Formula description	Physical meaning	Pump efficiency	Efficiency of the energy recovery device	Reference
$SEC = 2.05 \times 10^{-5} C_0 \frac{2-R}{2(1-R)} + 2.78 \times 10^{-7} \Delta P_{net}$	(22)	The cross flow structure and the RO device are considered.	RO treatment.	No consideration.	No consideration.	[12], [15]
$SEC = \frac{\pi_0}{1-R}$	(23)	The SEC does not include the energy required to create excess pressure in the module.	RO treatment.	No consideration.	No consideration.	[36]
$SEC = \sigma C_0 \left[\frac{1}{1-\alpha} + \frac{1-R}{R}\right] \frac{1}{\beta} \ln\left[\frac{1+(\beta-1)R}{1-R}\right]$	(24)	Intermittent reverse osmosis system.	RO treatment.	No consideration.	No consideration.	[37]
$SEC = \frac{P_f Q_f / \eta_{HP} - P_r Q_r \eta_{ERD}}{Q_p}$	(25)	The water flux and operating pressure during the dynamic operation of RO are considered.	RO treatment.	Included.	Included.	[38]
$SEC = \frac{Q_p P_f}{\eta_{HP}} + \frac{Q_{bp} P_{bp}}{\eta_{BP}} + \frac{Q_{in} P_{intake}}{\eta_{intake}}$	(26)	The water flux and operating pressure during the dynamic operation of RO are considered.	Total energy consumption for fresh water production.	Included.	Included.	[39]
$SEC = \frac{Q_f P_f C_0 g}{\eta_m \eta_{HP} Q_p}$	(27)	The water flux and operating pressure during the dynamic operation of RO are considered.	HPP and asynchronous motor.	Included.	No consideration.	[5]
$SEC = \frac{1}{1-R} + \varepsilon$	(28)	Specific energy consumption after normalization.	RO treatment.	No consideration.	No consideration.	[40], [41]
$SEC = \frac{1}{R}\left[\frac{P_f - P_p}{\eta_{HP}}\right] + (1-\beta_{ERD})\left[\frac{1-R}{R}\right] \times \left[\frac{P_p + \eta_{ERD}(P_f - P_r) - \eta_{ERD} P_f}{\eta_{HP}}\right]$	(29)	The leakage flow of ERD is considered.	RO treatment.	Included.	Included.	[18], [21]
$SEC = \frac{\frac{P_{f(plant)} \times 101325 \times Q_{f(plant)}}{Q_{p(plant)} \eta_p}}{36 \times 10^5}$	(30)	The water flux and operating pressure during the dynamic operation of RO are considered.	Total energy consumption for fresh water production.	Implicit.	Implicit.	[42]
$SEC = \frac{(1-\eta_{ERD}(1-Y_{SP}))}{\eta_P Y_{SP}} (P_f - P_0)$	(31)	The osmotic pressure of feed water is considered.	RO treatment.	Included.	Included.	[43]
$SEC = \frac{\dot{W}_{in}}{3600 \sum_{out} \dot{Q}_p}$	(32)	The SEC is obtained by dividing the total energy consumption of SWRO by the total water production volume.	Total energy consumption for fresh water production.	Implicit.	Implicit.	[44], [45]
$SEC = \frac{Q_{HP} g p \rho_f}{3.6 \times 10^6 \eta_m \eta_{HP}} + \frac{Q_{BP} g p \rho_f}{3.6 \times 10^6 \eta_m \eta_{BP}}$	(33)	The energy consumption of the high-pressure pump and booster pump is calculated, respectively.	RO treatment.	Included.	No consideration.	[46]
$SEC = \frac{1}{R} \int_0^R \left(\frac{J_w}{A} + e^{J_w/k} \frac{P_f}{1-RR'}\right) dRR'$	(34)	Constant finite flux is considered.	RO treatment.	No consideration.	No consideration.	[47]
$SEC = \frac{\Delta p_{avg} \Delta Q_D}{36 (Q_{D,in} + Q_{F,in})}$	(35)	The water flux and operating pressure during the dynamic operation of RO are considered.	RO treatment.	No consideration.	No consideration.	[48]

However, when the power frequency is variable, given a certain recovery rate, the SEC of RO desalination may be different due to the different power frequencies, especially for BWRO. This provides a way to reduce the energy consumption of RO desalination.However, reducing energy consumption by reducing frequency at the expense of fresh water production speed (Figure 7). Therefore, it is necessary to fully respect the water demand to reduce energy consumption in this way.

C. EXPERIMENT SUMMARY

Figure 7 to Figure 12 analyze how the power frequency and operating pressure affect the permeate flow, brine discharge, permeate quality, total energy consumption, recovery rate and SEC of RO desalination. Properly adjusting the VFD and pressure regulating valve can reduce the power consumption as much as possible on the premise of meeting the demand of water production. The experimental results show that the decrease in power frequency can reduce the feed water flow by reducing the HPP speed, which can improve the recovery rate and reduce the SEC. However, the operating pressure does not change the feed water flow. The pressure regulating valve improves the recovery rate and reduces the SEC by limiting the brine flow. In addition, the variation in the key parameters in RO desalination is shown in Figure 16.

IV. CONCLUSION

The application of the VFD in RO desalination has a certain impact on the water production efficiency, power consumption and recovery rate. First, this paper analyzes the influence of the power frequency and operating pressure on the operation state of RO desalination through experiments. Then, the working principle of the VFD and pressure regulating valve in changing the energy consumption of RO desalination is discussed. Finally, it is pointed out that the actual SEC of RO desalination cannot be calculated according to the recovery rate when the power frequency is unknown. The specific conclusions are listed as follows:

- The feed water flow is only related to the power frequency but not to the operating pressure.
- Increasing the operating pressure and power frequency can both improve the permeate quality.

- When the power frequency is adjusted below the industrial frequency through VFD, the output voltage increases with the increase of power frequency. At this time, the permeate flow rate is increased, and the salt water discharge rate is faster, resulting in a decrease in the recovery rate.
- When the pressure regulating valve is used to increase the working pressure, the current increases with the increase of motor torque, so the total power consumption also increases, but the SEC decreases.
- Only when the power frequency is determined there be a one-to-one functional relationship between the recovery rate and SEC.

This paper is only a preliminary experimental study on the influence of the power frequency on RO desalination. We hope that the work in this paper can help the staff of RO desalination plants. In addition, we hope that we will continue to perform more detailed research on the process of calculating energy consumption in the future.

DECLARATION OF COMPETING INTEREST

The authors declare that they have no known competing financial interests or personal relationships that could have influenced the work reported in this paper.

APPENDIX A

In different application scenarios, the calculation formula of specific energy consumption is shown in Table 6.

REFERENCES

[1] N. Sawaki and C.-L. Chen, "Cost evaluation for a two-staged reverse osmosis and pressure retarded osmosis desalination process," *Desalination*, vol. 497, Jan. 2021, Art. no. 114767. [Online]. Available: http://www.sciencedirect.com/science/article/pii/S0011916420314454

[2] X. Liao, Y. Ren, L. Shen, T. Shu, H. He, and J. Wang, "A 'carrier-load' perspective method for investigating regional water resource carrying capacity," *J. Cleaner Prod.*, vol. 269, Oct. 2020, Art. no. 122043. [Online]. Available: http://www.sciencedirect.com/science/article/pii/S0959652620320904

[3] D. Zou and H. Cong, "Evaluation and influencing factors of China's industrial water resource utilization efficiency from the perspective of spatial effect," *Alexandria Eng. J.*, vol. 60, no. 1, pp. 173–182, Feb. 2021. [Online]. Available: http://www.sciencedirect.com/science/article/pii/S1110016820303203

[4] S. Tadadjeu, H. Njangang, P. Ningaye, and M. Nourou, "Linking natural resource dependence and access to water and sanitation in African countries," *Resour. Policy*, vol. 69, Dec. 2020, Art. no. 101880. [Online]. Available: http://www.sciencedirect.com/science/article/pii/S0301420720309119

[5] S. A. Urrea, F. D. Reyes, B. P. Suárez, and J. A. de la Fuente Bencomo, "Technical review, evaluation and efficiency of energy recovery devices installed in the Canary islands desalination plants," *Desalination*, vol. 450, pp. 54–63, Jan. 2019. [Online]. Available: http://www.sciencedirect.com/science/article/pii/S0011916417314510

[6] A. Ruiz-García, I. Nuez, M. D. Carrascosa-Chisvert, and J. J. Santana, "Simulations of BWRO systems under different feedwater characteristics. Analysis of operation windows and optimal operating points," *Desalination*, vol. 491, Oct. 2020, Art. no. 114582. [Online]. Available: http://www.sciencedirect.com/science/article/pii/S0011916420307207

[7] A. Ruiz-García and I. Nuez, "Long-term intermittent operation of a full-scale BWRO desalination plant," *Desalination*, vol. 489, Sep. 2020, Art. no. 114526. [Online]. Available: http://www.sciencedirect.com/science/article/pii/S0011916420305403

[8] M. A. Abdelkareem, M. E. H. Assad, E. T. Sayed, and B. Soudan, "Recent progress in the use of renewable energy sources to power water desalination plants," *Desalination*, vol. 435, pp. 97–113, Jun. 2018. [Online]. Available: http://www.sciencedirect.com/science/article/pii/S0011916417321306

[9] M. T. Mito, X. Ma, H. Albuflasa, and P. A. Davies, "Reverse osmosis (RO) membrane desalination driven by wind and solar photovoltaic (PV) energy: State of the art and challenges for large-scale implementation," *Renew. Sustain. Energy Rev.*, vol. 112, pp. 669–685, Sep. 2019. [Online]. Available: http://www.sciencedirect.com/science/article/pii/S1364032119303995

[10] J. Eke, A. Yusuf, A. Giwa, and A. Sodiq, "The global status of desalination: An assessment of current desalination technologies, plants and capacity," *Desalination*, vol. 495, Dec. 2020, Art. no. 114633. [Online]. Available: http://www.sciencedirect.com/science/article/pii/S0011916420313114

[11] H. Nassrullah, S. F. Anis, R. Hashaikeh, and N. Hilal, "Energy for desalination: A state-of-the-art review," *Desalination*, vol. 491, Oct. 2020, Art. no. 114569. [Online]. Available: http://www.sciencedirect.com/science/article/pii/S0011916420310304

[12] F. Mohammadi, M. Sahraei-Ardakani, Y. M. Al-Abdullah, and G. T. Heydt, "Coordinated scheduling of power generation and water desalination units," *IEEE Trans. Power Syst.*, vol. 34, no. 5, pp. 3657–3666, Sep. 2019.

[13] A. Al-Karaghouli and L. L. Kazmerski, "Energy consumption and water production cost of conventional and renewable-energy-powered desalination processes," *Renew. Sustain. Energy Rev.*, vol. 24, pp. 343–356, Aug. 2013. [Online]. Available: http://www.sciencedirect.com/science/article/pii/S1364032113000208

[14] N. Voutchkov, "Energy use for membrane seawater desalination–current status and trends," *Desalination*, vol. 431, pp. 2–14, Apr. 2018. [Online]. Available: http://www.sciencedirect.com/science/article/pii/S0011916417321057

[15] C. Liu, K. Rainwater, and L. Song, "Energy analysis and efficiency assessment of reverse osmosis desalination process," *Desalination*, vol. 276, nos. 1–3, pp. 352–358, Aug. 2011. [Online]. Available: http://www.sciencedirect.com/science/article/pii/S0011916411003031

[16] L. F. Greenlee, D. F. Lawler, B. D. Freeman, B. Marrot, and P. Moulin, "Reverse osmosis desalination: Water sources, technology, and today's challenges," *Water Res.*, vol. 43, no. 9, pp. 2317–2348, May 2009. [Online]. Available: http://www.sciencedirect.com/science/article/pii/S0043135409001547

[17] M. A. Alghoul, P. Poovanaesvaran, K. Sopian, and M. Y. Sulaiman, "Review of brackish water reverse osmosis (BWRO) system designs," *Renew. Sustain. Energy Rev.*, vol. 13, no. 9, pp. 2661–2667, Dec. 2009. [Online]. Available: http://www.sciencedirect.com/science/article/pii/S1364032109000690

[18] A. J. Karabelas, C. P. Koutsou, M. Kostoglou, and D. C. Sioutopoulos, "Analysis of specific energy consumption in reverse osmosis desalination processes," *Desalination*, vol. 431, pp. 15–21, Apr. 2018. [Online]. Available: http://www.sciencedirect.com/science/article/pii/S0011916417302862

[19] K. H. Chu, J. Lim, S.-J. Kim, T.-U. Jeong, and M.-H. Hwang, "Determination of optimal design factors and operating conditions in a large-scale seawater reverse osmosis desalination plant," *J. Cleaner Prod.*, vol. 244, Jan. 2020, Art. no. 118918. [Online]. Available: https://www.sciencedirect.com/science/article/pii/S0959652619337886

[20] K. G. Nayar, J. Fernandes, R. K. McGovern, K. P. Dominguez, A. McCance, B. S. Al-Anzi, and J. H. Lienhard, "Cost and energy requirements of hybrid RO and ED brine concentration systems for salt production," *Desalination*, vol. 456, pp. 97–120, Apr. 2019. [Online]. Available: https://www.sciencedirect.com/science/article/pii/S0011916418312761

[21] C. P. Koutsou, E. Kritikos, A. J. Karabelas, and M. Kostoglou, "Analysis of temperature effects on the specific energy consumption in reverse osmosis desalination processes," *Desalination*, vol. 476, Feb. 2020, Art. no. 114213. [Online]. Available: http://www.sciencedirect.com/science/article/pii/S0011916419315607

[22] S. Cordoba, A. Das, J. Leon, J. M. Garcia, and D. M. Warsinger, "Double-acting batch reverse osmosis configuration for best-in-class efficiency and low downtime," *Desalination*, vol. 506, Jun. 2021, Art. no. 114959. [Online]. Available: https://www.sciencedirect.com/science/article/pii/S0011916421000308

[23] Q. J. Wei, C. I. Tucker, P. J. Wu, A. M. Trueworthy, E. W. Tow, and J. H. Lienhard, "Impact of salt retention on true batch reverse osmosis energy consumption: Experiments and model validation," *Desalination*, vol. 479, Apr. 2020, Art. no. 114177. [Online]. Available: https://www.sciencedirect.com/science/article/pii/S0011916419314626

[24] R. Camoirano and G. Dellepiane, "Variable frequency drives for MSF desalination plant and associated pumping stations," *Desalination*, vol. 182, nos. 1–3, pp. 53–65, Nov. 2005. [Online]. Available: https://www.sciencedirect.com/science/article/pii/S0011916405004194

[25] J. Veza, B. Peñate, and F. Castellano, "Electrodialysis desalination designed for off-grid wind energy," *Desalination*, vol. 160, no. 3, pp. 211–221, Jan. 2004. [Online]. Available: https://www.sciencedirect.com/science/article/pii/S0011916404900240

[26] A. Ghobeity and A. Mitsos, "Optimal time-dependent operation of seawater reverse osmosis," *Desalination*, vol. 263, nos. 1–3, pp. 76–88, Nov. 2010. [Online]. Available: https://www.sciencedirect.com/science/article/pii/S0011916410004339

[27] M. G. Ahunbay, "Achieving high water recovery at low pressure in reverse osmosis processes for seawater desalination," *Desalination*, vol. 465, pp. 58–68, Sep. 2019. [Online]. Available: https://www.sciencedirect.com/science/article/pii/S0011916419300931

[28] I. de la Nuez Pestana, F. J. G. Latorre, C. A. Espinoza, and A. G. Gotor, "Optimization of RO desalination systems powered by renewable energies—Part I: Wind energy," *Desalination*, vol. 160, no. 3, pp. 293–299, Jan. 2004. [Online]. Available: https://www.sciencedirect.com/science/article/pii/S0011916404900318

[29] M. S. Miranda and D. Infield, "A wind-powered seawater reverse-osmosis system without batteries," *Desalination*, vol. 153, nos. 1–3, pp. 9–16, Feb. 2003. [Online]. Available: https://www.sciencedirect.com/science/article/pii/S0011916402010883

[30] M. Thomson, M. S. Miranda, and D. Infield, "A small-scale seawater reverse-osmosis system with excellent energy efficiency over a wide operating range," *Desalination*, vol. 153, nos. 1–3, pp. 229–236, Feb. 2003. [Online]. Available: https://www.sciencedirect.com/science/article/pii/S0011916402011414

[31] E. S. Mohamed, G. Papadakis, E. Mathioulakis, and V. Belessiotis, "An experimental comparative study of the technical and economic performance of a small reverse osmosis desalination system equipped with an hydraulic energy recovery unit," *Desalination*, vol. 194, nos. 1–3, pp. 239–250, Jun. 2006. [Online]. Available: https://www.sciencedirect.com/science/article/pii/S0011916406003778

[32] A. Uppu, A. Chaudhuri, and S. P. Das, "Numerical modeling of particulate fouling and cake-enhanced concentration polarization in roto-dynamic reverse osmosis filtration systems," *Desalination*, vol. 468, Oct. 2019, Art. no. 114053. [Online]. Available: https://www.sciencedirect.com/science/article/pii/S0011916418326304

[33] F. J. Millero, R. Feistel, D. G. Wright, and T. J. McDougall, "The composition of standard seawater and the definition of the reference-composition salinity scale," *Deep Sea Res. I, Oceanogr. Res. Papers*, vol. 55, no. 1, pp. 50–72, Jan. 2008. [Online]. Available: https://www.sciencedirect.com/science/article/pii/S0967063707002282

[34] S. V. Giannoutsos and S. N. Manias, "A data-driven process controller for energy-efficient variable-speed pump operation in the central cooling water system of marine vessels," *IEEE Trans. Ind. Electron.*, vol. 62, no. 1, pp. 587–598, Jan. 2015.

[35] D.-H. Hellmann, H. Rosenberger, and E. F. Tusel, "Saving of energy and cost in seawater desalination with speed controlled pumps," *Desalination*, vol. 139, nos. 1–3, pp. 7–19, Sep. 2001. [Online]. Available: https://www.sciencedirect.com/science/article/pii/S0011916401002909

[36] S. Lin and M. Elimelech, "Staged reverse osmosis operation: Configurations, energy efficiency, and application potential," *Desalination*, vol. 366, pp. 9–14, Jun. 2015. [Online]. Available: http://www.sciencedirect.com/science/article/pii/S0011916415001393

[37] T. Y. Qiu and P. A. Davies, "Longitudinal dispersion in spiral wound RO modules and its effect on the performance of batch mode RO operations," *Desalination*, vol. 288, pp. 1–7, Mar. 2012. [Online]. Available: http://www.sciencedirect.com/science/article/pii/S0011916411010009

[38] A. Jiang, J. Wang, L. T. Biegler, W. Cheng, C. Xing, and Z. Jiang, "Operational cost optimization of a full-scale SWRO system under multi-parameter variable conditions," *Desalination*, vol. 355, pp. 124–140, Jan. 2015. [Online]. Available: http://www.sciencedirect.com/science/article/pii/S0011916414005396

[39] A. A. Atia and V. Fthenakis, "Active-salinity-control reverse osmosis desalination as a flexible load resource," *Desalination*, vol. 468, Oct. 2019, Art. no. 114062. [Online]. Available: http://www.sciencedirect.com/science/article/pii/S0011916419306770

[40] F. E. Ahmed, R. Hashaikeh, A. Diabat, and N. Hilal, "Mathematical and optimization modelling in desalination: State-of-the-art and future direction," *Desalination*, vol. 469, Nov. 2019, Art. no. 114092. [Online]. Available: http://www.sciencedirect.com/science/article/pii/S0011916419312366

[41] S. Lin and M. Elimelech, "Kinetics and energetics trade-off in reverse osmosis desalination with different configurations," *Desalination*, vol. 401, pp. 42–52, Jan. 2017. [Online]. Available: http://www.sciencedirect.com/science/article/pii/S0011916416312656

[42] M. A. Al-Obaidi, G. Filippini, F. Manenti, and I. M. Mujtaba, "Cost evaluation and optimisation of hybrid multi effect distillation and reverse osmosis system for seawater desalination," *Desalination*, vol. 456, pp. 136–149, Apr. 2019. [Online]. Available: http://www.sciencedirect.com/science/article/pii/S0011916418319441

[43] T. Lee, A. Rahardianto, and Y. Cohen, "Flexible reverse osmosis (flero) desalination," *Desalination*, vol. 452, pp. 123–131, 2019. [Online]. Available: http://www.sciencedirect.com/science/article/pii/S0011916418317193

[44] M. A. Jamil, B. A. Qureshi, and S. M. Zubair, "Exergo-economic analysis of a seawater reverse osmosis desalination plant with various retrofit options," *Desalination*, vol. 401, pp. 88–98, Jan. 2017. [Online]. Available: http://www.sciencedirect.com/science/article/pii/S0011916418317193

[45] B. A. Qureshi and S. M. Zubair, "Exergetic analysis of a brackish water reverse osmosis desalination unit with various energy recovery systems," *Energy*, vol. 93, pp. 256–265, Dec. 2015. [Online]. Available: http://www.sciencedirect.com/science/article/pii/S0360544215011895

[46] D. R. Prathapaneni and K. Detroja, "Optimal design of energy sources and reverse osmosis desalination plant with demand side management for cost-effective freshwater production," *Desalination*, vol. 496, Dec. 2020, Art. no. 114741. [Online]. Available: http://www.sciencedirect.com/science/article/pii/S0011916420314193

[47] Y. Okamoto and J. H. Lienhard, "How RO membrane permeability and other performance factors affect process cost and energy use: A review," *Desalination*, vol. 470, Nov. 2019, Art. no. 114064. [Online]. Available: http://www.sciencedirect.com/science/article/pii/S0011916419305752

[48] J. Benjamin, M. E. Arias, and Q. Zhang, "A techno-economic process model for pressure retarded osmosis based energy recovery in desalination plants," *Desalination*, vol. 476, Feb. 2020, Art. no. 114218. [Online]. Available: http://www.sciencedirect.com/science/article/pii/S0011916419315115

SHUAI CHU was born in Baotou, Inner Mongolia, China, in 1993. He received the B.S. degree from the School of Science, Northeast Electric Power University, in 2016, and the M.S. degree from the School of Electrical Engineering, Northeast Electric Power University, in 2019. He is currently pursuing the Ph.D. degree with the School of Electrical Engineering, Shenyang University of Technology. His research interest is the technology of combining clean energy with seawater desalination.

SHITAN ZHANG was born in Shenyang, Liaoning, China, in 1998. She received the B.S. degree from the School of Electrical Engineering, Northeast Electric Power University, in 2020, where she is currently pursuing the M.S. degree. Her research interest is the energy saving technology of seawater reverse osmosis.

XIAONA MA received the Ph.D. degree in environmental engineering and the Ph.D. degree from the Institute of Oceanology, Chinese Academy of Sciences, in 2018 and 2021, respectively. Her current research interests include harmless treatment and resource utilization of aquaculture tail water, and sea water desalination.

YINXUAN LI was born in Harbin, Heilongjiang, China, in 1995. She received the B.S. and M.S. degrees from the School of Electrical Engineering, Northeast Electric Power University, in 2017 and 2020, respectively. She is with the State Grid Tianjin Marketing Service Center (Metrology Center). Her research interest is the technology of combining clean energy with seawater desalination.

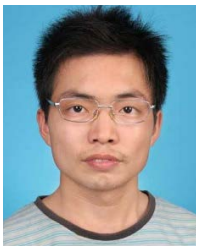

DENGGAO QIU received the M.Sc. degree in aquaculture from Southwest University, Chongqing, China, in 2009, and the Ph.D. degree in marine ecology from the Institute of Oceanology, Chinese Academy of Sciences, in 2014. He is a Research Associate with the Fisheries Research Institute of Fujian, Xiamen, China. His current research interests include harmless treatment and resource utilization of aquaculture tail water, and sea water desalination.

WEICHUN GE was born in Shenyang, Liaoning, China, in 1961. He received the M.S. degree from the School of Electrical Engineering, Northeast Electric Power University, in 1987, and the Ph.D. degree from the School of Electrical Engineering, North China Electric Power University, in 1992. Since 2007, he has been receiving the special government allowance from the state council. His research interests include the energy saving technology of seawater reverse osmosis and demand response of power grid. He has won the title of Liaoning Outstanding Scientific and Technological Worker, in 2017. He has also won the National Science and Technology Progress Award five times in total.

LEI KOU received the M.Sc. degree in computer science and technology and the Ph.D. degree in electrical engineering from Northeast Electric Power University, Jilin, China, in 2017 and 2020, respectively. He is a Research Associate with the Institute of Oceanographic Instrumentation, Shandong Academy of Sciences. His current research interests include fault diagnosis, artificial intelligence, machine learning, and power electronic technology.